Myelin suppresses axon regeneration by PIR-B/SHP-mediated inhibition of Trk activity

Yuki Fujita[1,2], Shota Endo[3],
Toshiyuki Takai[3] and
Toshihide Yamashita[1,2,*]

[1]Department of Molecular Neuroscience, Graduate School of Medicine, Osaka University, Osaka, Japan, [2]JST, CREST, Tokyo, Japan and [3]Department of Experimental Immunology and CREST Program of JST, Institute of Development, Aging and Cancer, Tohoku University, Sendai, Japan

Paired immunoglobulin-like receptor B (PIR-B) partially mediates the regeneration-inhibiting effects of the myelin-derived protein Nogo, myelin-associated glycoprotein (MAG), and oligodendrocyte-myelin glycoprotein (OMgp). In this study, we report that inhibition of the PIR-B signaling cascades in neurons enhances axon regeneration in the central nervous system (CNS). Binding of MAG to PIR-B led to the association of PIR-B with tropomyosin receptor kinase (Trk) neurotrophin receptors. Src homology 2-containing protein tyrosine phosphatase (SHP)-1 and SHP-2, which were recruited to PIR-B upon MAG binding, functioned as Trk tyrosine phosphatases. Further, SHP-1 and SHP-2 inhibition reduced MAG-induced dephosphorylation of Trk receptors and abolished the inhibitory effect of MAG on neurite growth. Thus, PIR-B associated with Trk to downregulate basal and neurotrophin-regulated Trk activity through SHP-1/2 in neurons. Moreover, in vivo transfection of small interfering RNA (siRNA) for SHP-1 or SHP-2 induced axonal regeneration after optic nerve injury in mice. Our results thus identify a new molecular target to enhance regeneration of the injured CNS.

Introduction

Myelin-derived inhibitors of axonal regeneration have an important role in inhibiting regeneration in the adult central nervous system (CNS) (Yiu and He, 2006). Three myelin-derived proteins possess potent inhibitory activity for neurite growth in vitro by interacting with the Nogo receptor (NgR). However, in a previous in vitro study, researchers have reported that genetic deletion of NgR does not reduce neurite growth inhibition by myelin-derived proteins (Zheng et al, 2005). This observation suggested the existence of other hitherto unidentified binding receptors for these inhibitors. Later, paired immunoglobulin-like receptor B (PIR-B)—a major histocompatibility complex (MHC) class I receptor (Takai, 2005)—was identified as a second receptor (Atwal et al, 2008). PIR-B is expressed on various haematopoietic cells as well as on neurons (Syken et al, 2006). It binds not only to the 66-amino acid long Nogo-66, which is one of the two inhibitory domains of Nogo, but also to myelin-associated glycoprotein (MAG) and oligodendrocyte-myelin glycoprotein (OMgp). Further, the presence of PIR-B is essential for inhibition of neurite growth mediated by Nogo-66 and other myelin proteins (Atwal et al, 2008). It is unknown whether PIR-B inhibition promotes axonal regeneration after injury to the CNS in vivo. Nonetheless, the role of PIR-B in restricting plasticity during development is supported by the fact that deprivation-induced expansion of the open eye's territory is more robust and can be properly induced after the critical developmental period in mice expressing PIR-B lacking the transmembrane domain (PIR-B-TM mice) (Syken et al, 2006). Therefore, we considered that elucidating the molecular mechanism underlying PIR-B signaling in neurons should increase our knowledge on the inability of injured axons to regenerate as well as on the plasticity of the developing CNS.

PIR-B contains immunoreceptor tyrosine-based inhibitory motifs. Phosphorylation of these sites upon ligand binding leads to Src homology 2-containing protein tyrosine phosphatase (SHP)-1 and SHP-2 recruitment to PIR-B, which then modulates immune signal transduction pathways. PIR-B isolated from the brain is also phosphorylated and associated with SHP-1 and SHP-2 (Syken et al, 2006). Thus, it would be of interest to elucidate the signaling mechanism of PIR-B in neurons by determining whether SHP phosphatase recruitment occurs upon ligand stimulation and to clarify whether SHP mediates PIR-B signaling in neurons. Thus, we aimed to identify the molecular targets of SHP-1 and SHP-2. SHP-1 has been shown to interact with and dephosphorylate several growth factor receptors, including insulin-like growth factor-1 (IGF-1), platelet-derived growth factor (PDGF), and epidermal growth factor (EGF) receptors (Tonks and Neel, 2001). Interestingly, a previous study reported that SHP-1 dephosphorylates the tropomyosin receptor kinase A (TrkA) receptor, a nerve growth factor (NGF) receptor, in PC12 cells and sympathetic neurons. Further, an enhanced association of SHP-2 with the TrkB receptor—a brain-derived neurotrophic factor (BDNF) receptor—inhibits BDNF-induced TrkB autophosphorylation and activation in cerebellar neurons (Rusanescu et al, 2005). These findings prompted us to hypothesize that Trk receptors are PIR-B targets in neurons (Marsh et al, 2003).

In the present study, we demonstrated that PIR-B binds to and inactivates Trk neurotrophin receptors, which are known to promote neurite growth in neurons. Upon MAG activation, PIR-B recruited SHP-1 and SHP-2, which in turn dephosphorylated the Trk receptors. We suggest that reduced Trk receptor activity results in MAG-induced neurite growth inhibition. Further, the inhibition of SHP promoted axonal regeneration of the injured optic nerve *in vivo*.

Results

Trk receptors are PIR-B targets

We first examined whether PIR-B interacted with Trk receptors. COS-7 cells were transfected with haemagglutinin (HA)-tagged full-length TrkB (HA–TrkB FL) and/or full-length PIR-B constructs. The cell extracts were immunoprecipitated with anti-PIR-B or anti-HA antibodies (Figure 1A and B). Of
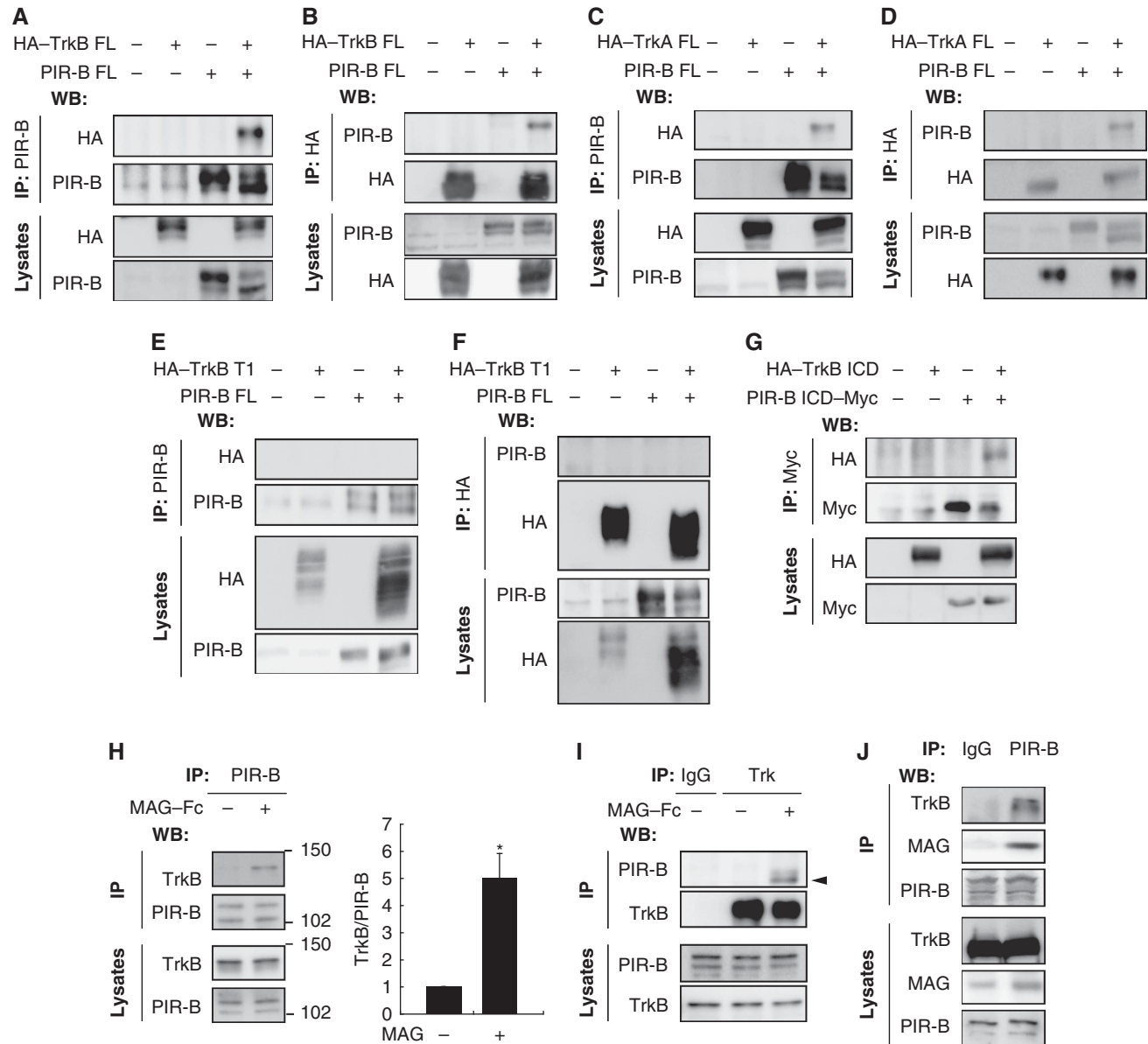
Figure 1 Ligand-dependent association of PIR-B with TrkB. (**A**, **B**) Co-immunoprecipitation of full-length PIR-B (PIR-B FL) with HA-tagged full-length TrkB (HA–TrkB FL). COS-7 cells were transiently transfected with the indicated plasmids. Cell lysates were immunoprecipitated with anti-PIR-B (**A**) or anti-HA (**B**) antibodies. The immunoprecipitates (IP) and cell lysates (lysates) were analysed by immunoblotting with anti-HA and anti-PIR-B antibodies. (**C**, **D**) Co-immunoprecipitation of PIR-B FL with HA-tagged full-length TrkA (HA–TrkA FL). COS-7 cells were transiently transfected with the indicated plasmids. Cell lysates were immunoprecipitated with anti-PIR-B (**C**) or anti-HA (**D**) antibodies. Western blotting was performed using the indicated antibodies. (**E**, **F**) PIR-B and HA-tagged TrkB T1 did not interact in the transfected COS-7 cells. Co-immunoprecipitation was carried out as shown in (**A**, **B**). (**G**) Co-immunoprecipitation of Myc-tagged PIR-B ICD (PIR-B ICD–Myc) with HA-tagged TrkB ICD (HA–TrkB ICD) using anti-Myc antibodies. (**H**, **I**) Association of endogenous PIR-B with TrkB in CGNs. CGNs were left untreated or were treated with MAG–Fc (25 µg/ml) for 15 min. Lysates prepared from the CGNs were immunoprecipitated with anti-PIR-B (**H**) or anti-pan Trk (**I**) antibodies, followed by immunoblotting with anti-TrkB and anti-PIR-B antibodies, respectively. The association between PIR-B and TrkB was observed in MAG-treated cells. IgG, control IgG. The arrowhead indicates the band corresponding to PIR-B. The TrkB signal intensity was quantified by densitometry and normalized to the signal intensity of precipitated PIR-B (**H**). *$P < 0.05$ by Welch's *t*-test. (**J**) Interaction of PIR-B with TrkB and MAG in the mouse brain. Lysates prepared from whole mouse brain were immunoprecipitated with anti-PIR-B antibodies, followed by western blotting for TrkB and MAG.

these, HA–TrkB was detected only in the HA–TrkB–PIR-B co-transfected cells precipitated with anti-PIR-B antibodies (Figure 1A). These results were consistent with those for HA–TrkB immunoprecipitation with anti-HA antibodies (Figure 1B). These findings demonstrated that ectopically expressed PIR-B interacted with TrkB in COS-7 cells. Assessment of the association of full-length TrkA and PIR-B yielded identical results (Figure 1C and D). We then investigated the molecular determinants of the PIR-B–TrkB interaction. COS-7 cells were transfected with a HA-tagged deletion construct of TrkB (HA–TrkB T1) lacking most of the intracellular domains and/or full-length PIR-B constructs (Figure 1E and F). Immunoprecipitation of the transfected cells with anti-PIR-B (Figure 1E) or anti-HA (Figure 1F) antibodies revealed no association between HA–TrkB T1 and PIR-B. Next, COS-7 cells were transfected with HA-tagged TrkB intracellular domain (HA–TrkB ICD) or PIR-B ICD. We found an interaction between HA–TrkB ICD and PIR-B ICD (Figure 1G), indicating that PIR-B associated with TrkB intracellularly, rather than extracellularly, in the transfected cells. Cell lysates expressing TrkB and PIR-B were prepared from mouse cerebellar granule neurons (CGNs) obtained on postnatal day (P) 7. A previous study has demonstrated that PIR-B is required for neurite growth inhibition in CGNs (Atwal *et al*, 2008). The cells were immunoprecipitated with anti-PIR-B antibodies and immunoblotted using anti-TrkB antibodies. TrkB was detected in the immunoprecipitates obtained using an anti-TrkB antibody after the cells were stimulated with 25 µg/ml MAG for 15 min (Figure 1H). Immunoprecipitation with an anti-TrkB or control antibody followed by immunoblotting with anti-PIR-B antibodies also yielded similar results (Figure 1I). Thus, interaction of PIR-B with TrkB in CGNs is ligand dependent. We further assessed the interaction between these proteins using lysates prepared from P7 brains. As expected, PIR-B was co-immunoprecipitated with TrkB and MAG (Figure 1J).

Association of SHP with PIR-B and TrkB

PIR-B is phosphorylated upon ligand binding and triggers the recruitment of SHP-1 and SHP-2 to PIR-B in immune cells (Takai, 2005). We evaluated the involvement of SHP in MAG signaling. CGNs were used to identify the possible association between PIR-B and SHP-2. Both SHP-2 (Figure 2A) and SHP-1 (Figure 4C) were expressed in the CGNs. The cell lysates were immunoprecipitated with an anti-PIR-B antibody or control IgG, and western blotting was performed to detect SHP-2. The association between SHP-2 and PIR-B was enhanced by MAG–Fc treatment (Figure 2A). SHP-2 immunoprecipitation yielded consistent results (Figure 2B), indicating the ligand-dependent enhancement of the PIR-B–SHP-2 interaction in CGNs. We then investigated whether TrkB associated with SHP-1 or SHP-2. COS-7 cells were transfected with HA–TrkB and PIR-B and left untreated or treated with MAG–Fc for 15 min, followed by immunoprecipitation with anti-TrkB or control IgG. SHP-2 was co-immunoprecipitated with TrkB; this association was enhanced by MAG–Fc treatment (Figure 2C). Identical results were obtained in CGNs (Figure 2D). In addition, we assessed the ligand-dependent recruitment of SHPs to PIR-B and TrkB in CGNs. Both SHP-2 and TrkB were co-immunoprecipitated with PIR-B after MAG–Fc treatment (Figure 2E). These results demon-

strate that SHP-2 was recruited to PIR-B and TrkB upon MAG stimulation.

MAG stimulation induces dephosphorylation of Trk receptors by an SHP-1- and SHP-2-dependent mechanism

To explore the physiological role of the PIR-B–TrkB–SHP complex, we performed loss-of-function experiments using small interfering RNA (siRNA). We first examined if transfection with these siRNAs specifically reduced the corresponding target mRNAs. siRNA nucleofection of CGNs yielded almost 100% transfection efficiency (data not shown). Efficient downregulation of *shp1* mRNA was found specifically in SHP-1 siRNA-transfected but not SHP-2 siRNA-transfected cells (Figure 3A; 87% inhibition by SHP-1 siRNA #1 and 72% inhibition by SHP-1 siRNA #2). Similarly, SHP-2 siRNA but not SHP-1 siRNA reduced *shp2* transcript levels (Figure 3B; 84% inhibition by SHP-2 siRNA #1 and 69% inhibition by SHP-2 siRNA #2). Consistent results were obtained when we assessed the protein expression levels in these siRNA-transfected cells (Figure 3C), indicating that we successfully achieved siRNA-mediated knockdown of SHP-1 and SHP-2.

We determined that PIR-B, Trk receptors, and SHP-2 interacted in response to MAG stimulation. We then tested whether SHPs regulated Trk receptor activity. The Trk receptors were immunoprecipitated with anti-pan Trk antibodies, followed by western blotting for phosphotyrosine to detect their phosphorylation status. The CGNs, which express PIR-B and TrkB endogenously, were treated with MAG–Fc for 30 min, followed by immunoprecipitation with anti-pan Trk antibodies. We did not detect phosphotyrosine signals in the CGNs (Figure 4A, left lane). However, this result did not imply that Trk receptors were completely inactive under baseline conditions in the absence of neurotrophins; rather, it suggested that the activity was below the detection threshold determined by the sensitivity of the antibodies used (Figure 5B and C). To raise the detection threshold, we added 100 ng/ml BDNF to the culture. In this condition, Trk receptors were tyrosine dephosphorylated upon treatment of CGNs with MAG–Fc (Figure 4A). We used the SHP inhibitor 8-hydroxy-7-(6-sulphonaphthalen-2-yl)diazenyl-quinoline-5-sulphonic acid (NSC-87877) to assess whether MAG–Fc-induced dephosphorylation of Trk receptors was dependent on SHP. Pretreatment of the CGNs with NSC-87877 for 3 h significantly reduced MAG–Fc-induced dephosphorylation (Figure 4B). We then knocked down SHP-1 or SHP-2 using siRNA. Knockdown of SHP-1 or SHP-2 with the corresponding siRNAs inhibited MAG–Fc-induced dephosphorylation of the Trk receptors (Figure 4C and D). Knockdown of either SHP-1 or SHP-2 was sufficient for complete suppression of the effect of MAG on the phosphorylation state of Trk receptors; therefore, both SHP-1 and SHP-2 or a certain amount of the total activity of both phosphatases may be required for MAG–Fc-induced Trk dephosphorylation.

We further tested whether SHPs regulate phosphorylation of Trk receptors in dissociated retinal neurons. TrkB was immunoprecipitated with anti-TrkB antibodies and the phosphorylation levels of TrkB were determined. Knockdown of either SHP-1 (Figure 4E) or SHP-2 (Figure 4F) abolished MAG-induced TrkB dephosphorylation in retinal cells.

Notably, knockdown of either SHP-1 (Figure 4E) or SHP-2 (Figure 4F) *per se* enhanced TrkB phosphorylation.

We used PIR-B$^{-/-}$ mice to determine the contribution of PIR-B to the inhibitory effect of MAG–Fc. PIR-B$^{-/-}$ mice lacking the sequences encoding the sixth ectodomain and juxtamembrane domains were generated by standard gene targeting methods (Ujike *et al*, 2002). MAG–Fc-induced dephosphorylation was lower in cells isolated from PIR-B$^{-/-}$
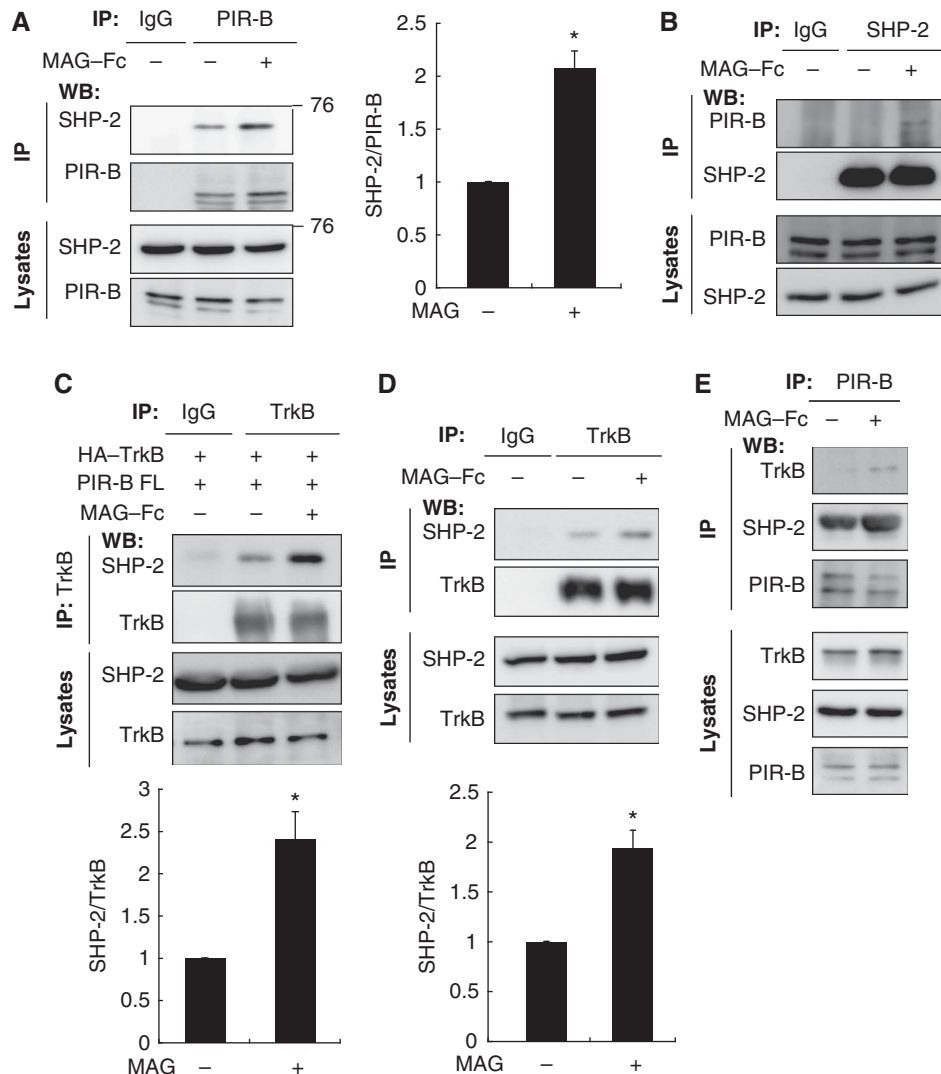

Figure 2 Co-immunoprecipitation of PIR-B with SHP-2. (**A**, **B**) Association of endogenous PIR-B with SHP-2 in CGNs. CGNs were left untreated or treated with MAG–Fc (25 µg/ml) for 15 min. The lysates were immunoprecipitated with anti-PIR-B (**A**) or anti-SHP-2 (**B**) antibodies, followed by western blotting analysis with anti-SHP-2 and anti-PIR-B antibodies, respectively. The interaction of PIR-B and SHP-2 was enhanced by treatment with MAG–Fc. The relative levels of SHP-2 were normalized to the signal intensity of the precipitated PIR-B (graph). *$P<0.05$ by Welch's *t*-test. (**C**) COS-7 cells were transfected with HA-tagged TrkB (HA–TrkB) and PIR-B, and left untreated or treated with MAG–Fc (25 µg/ml) for 15 min. The lysates were immunoprecipitated with an anti-TrkB antibody or control IgG. Association of HA–TrkB with SHP-2 was enhanced by treatment with MAG–Fc. The relative levels of SHP-2 after immunoprecipitation with TrkB are shown (graph). (**D**) CGNs were left untreated or treated with MAG–Fc (25 µg/ml) for 15 min. The lysates were immunoprecipitated with an anti-TrkB antibody or control IgG. Association of TrkB with SHP-2 was enhanced by treatment with MAG–Fc. The relative levels of SHP-2 after immunoprecipitation with TrkB are shown (graph). *$P<0.05$ by Welch's *t*-test. (**E**) PIR-B associated with TrkB and SHP-2 upon stimulation of CGNs with MAG. CGNs treated with MAG–Fc for 15 min were lysed and immunoprecipitated with an anti-PIR-B antibody, and the precipitated proteins were detected using western blotting with anti-PIR-B, anti-TrkB, and anti-SHP-2 antibodies.

Figure 3 siRNA-mediated knockdown of SHP mRNA and protein levels in CGNs. (**A**, **B**) SHP-1 and SHP-2 siRNA specifically reduced target mRNA expression. CGNs were transfected with the indicated siRNAs. Total RNA isolated at 72 h after transfection was analysed by real-time PCR. Transfection with SHP-1 siRNA reduced *shp1* transcript levels by 87% (SHP-1 siRNA #1) or 72% (SHP-1 siRNA #2) but did not affect *shp2* expression levels (**A**). Transfection with SHP-2 siRNA reduced *shp2* transcript levels by 84% (SHP-2 siRNA #1) or 69% (SHP-2 siRNA #2) but did not affect *shp1* expression levels (**B**). (**C**) SHP-1 and SHP-2 siRNA specifically reduced target protein expression. CGNs were transfected with the indicated siRNAs. Cell lysates were prepared 72 h after transfection and subjected to western blotting. (**D**, **E**) Transfection of SHP-1 (**D**) or SHP-2 (**E**) siRNA suppressed MAG-induced neurite outgrowth inhibition. The effect of MAG was rescued by co-transfection of the construct encoding SHP-1 (**D**) or SHP-2 (**E**). CGNs were transfected with the indicated siRNAs and/or expression vector. The transfected CGNs were cultured for 24 h in the presence or absence of MAG–Fc. The mean lengths of the longest neurite per neuron are shown in the graph. Representative western blots showing detection of SHP-1 (**D**) and SHP-2 (**E**) are presented (left panels). (**A–E**) **$P<0.01$, *$P<0.05$.

mice than in cells isolated from wild-type (WT) mice (Figure 4G), indicating that PIR-B is required for MAG–Fc-induced dephosphorylation of the Trk receptors.

We next investigated the contribution of the p75 receptor to MAG-induced TrkB dephosphorylation; p75 interacts with NgR to mediate MAG and Nogo-66 signal transduction
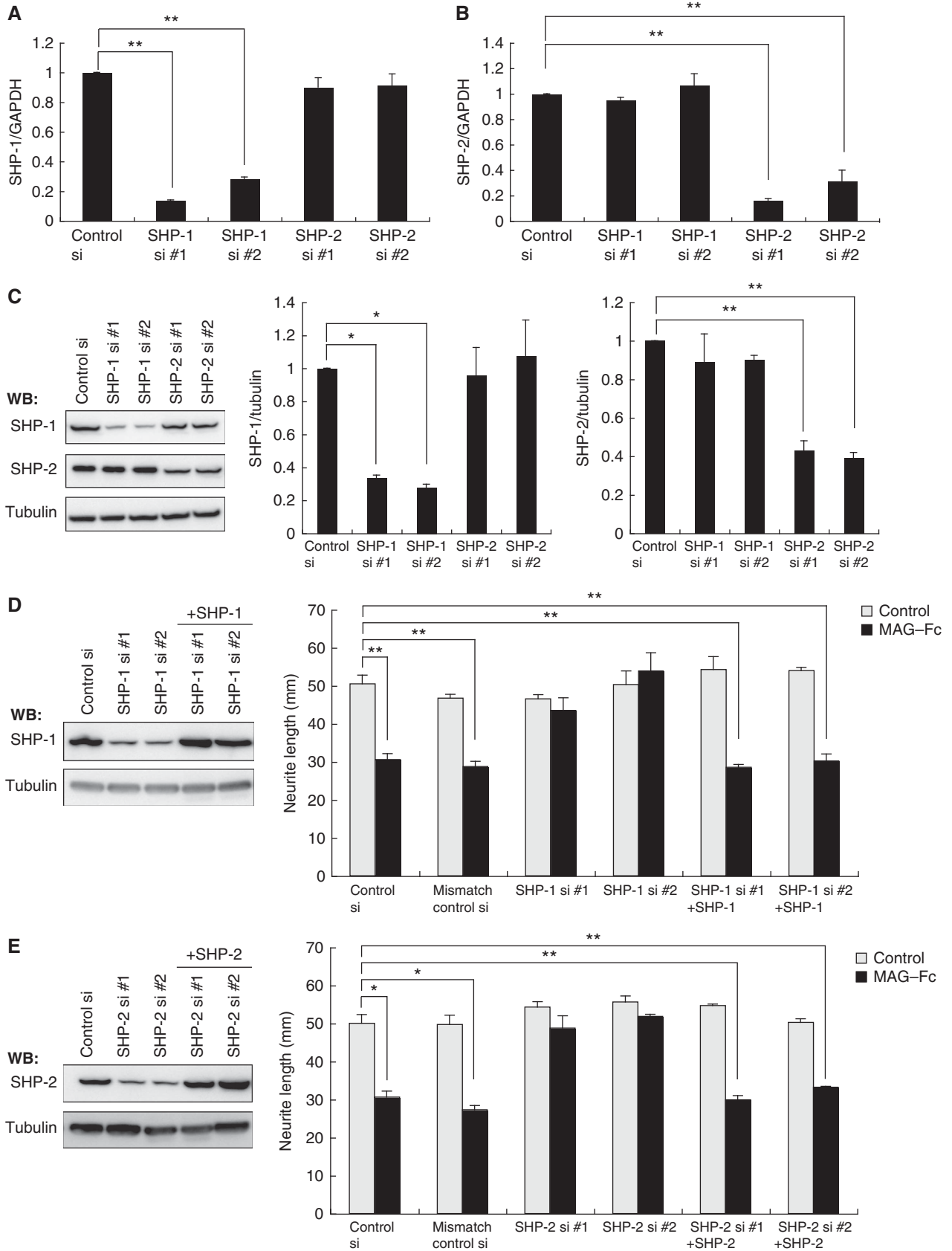
(Wang *et al*, 2002; Yamashita *et al*, 2002). In addition, p75 is a co-receptor of Trk receptors. To explore whether p75 is also required for PIR-B/TrkB signal transduction, we used CGNs isolated from mice carrying a mutation in the *p75* gene (Lee *et al*, 1992). Trk receptors of WT CGNs were tyrosine dephosphorylated upon MAG–Fc treatment. In contrast, no change was observed in CGNs isolated from mice bearing

the *p75* mutation (Figure 4H). Thus, p75 is required for MAG-induced tyrosine dephosphorylation of Trk receptors.
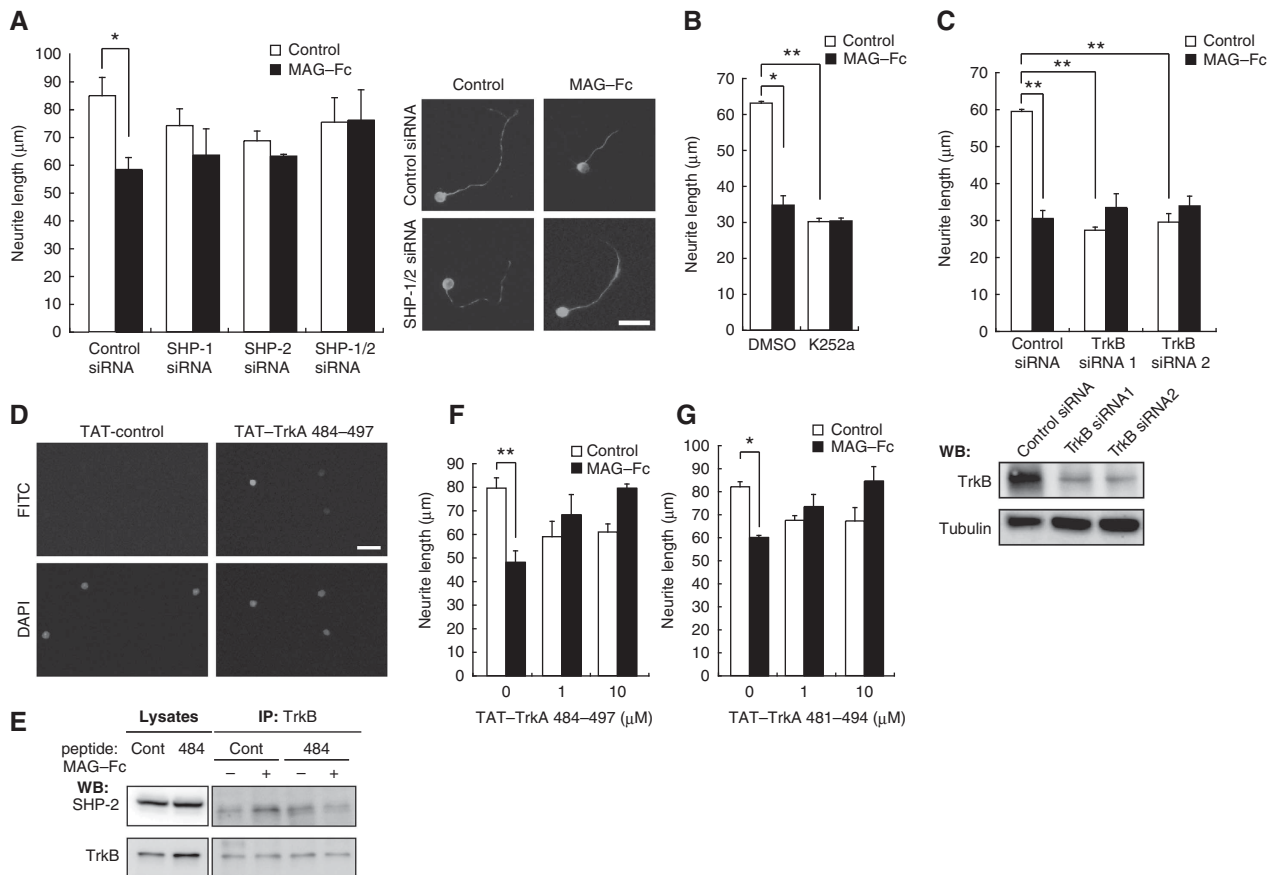
SHP-1 and SHP-2 are required for the inhibitory effect of MAG on neurite growth in CGNs

To assess the involvement of SHP in MAG-mediated neurite growth inhibition, we compared the neurite length
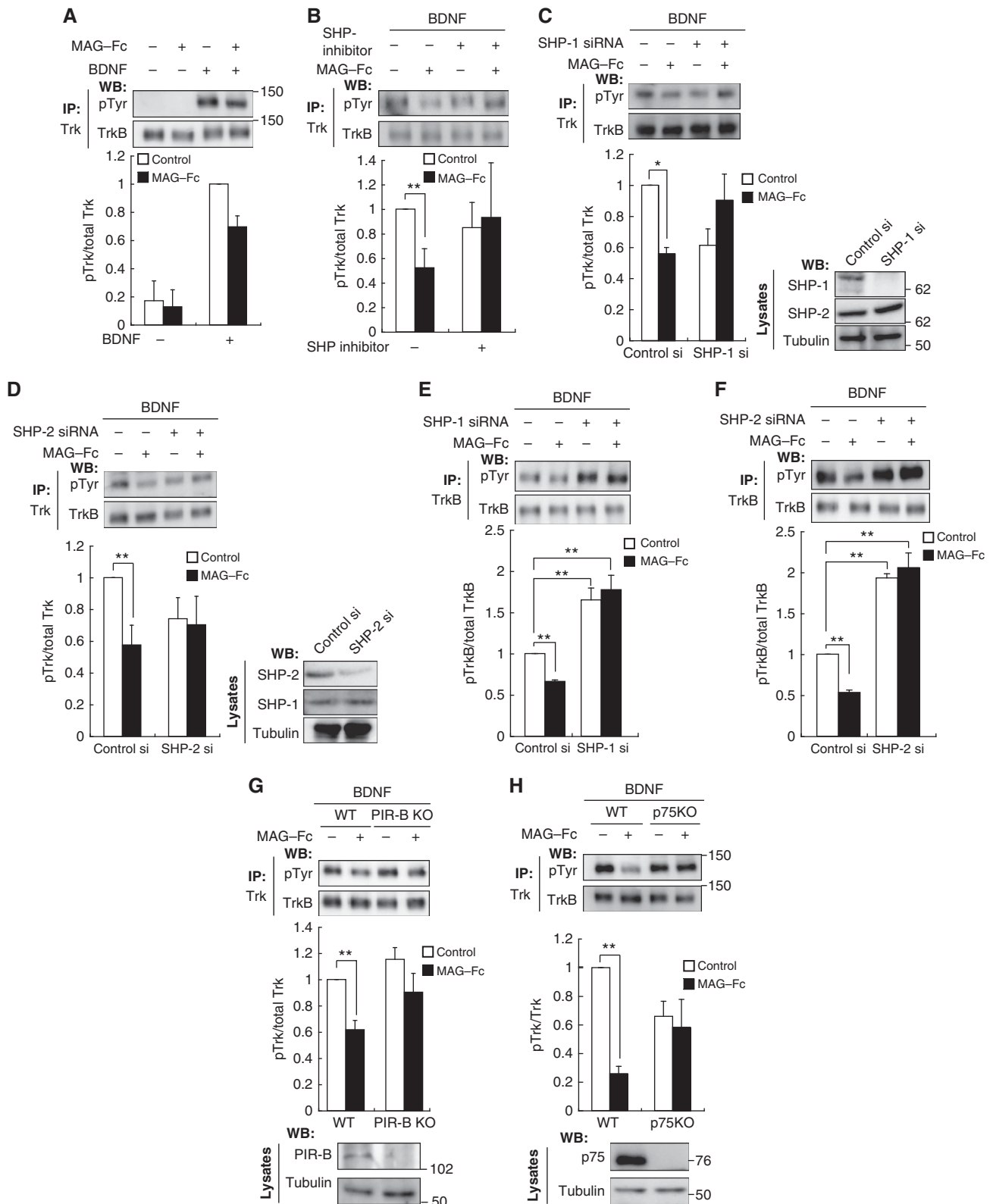
of MAG-treated and control neurons for 24 h. Neurite outgrowth in WT CGNs was significantly inhibited by MAG–Fc (Figure 5A). Using PIR-B$^{-/-}$ mice, we found that PIR-B was necessary for this effect (data not shown). This is in agreement with a previous study (Atwal et al, 2008).

Although knockdown of SHP-1 or SHP-2 did not promote neurite growth, it reduced the inhibitory effect of MAG–Fc (Figure 3D and E). We performed rescue experiments using the same neurite growth assay in CGNs. Transfection of SHP-1 or SHP-2 cDNA in a form refractory to siRNA restored

Figure 5 SHP and Trk receptors are required for the inhibitory effect of MAG. (**A**) siRNA-mediated knockdown of endogenous SHP-1 and SHP-2 suppressed the inhibitory effect of MAG–Fc on neurite growth. The transfected CGNs were cultured on poly-L-lysine-coated chamber slides for 24 h in the presence or absence of MAG–Fc. The mean lengths of the longest neurite per neuron are represented in the graph. The representative images of transfected CGNs are shown. Scale bar: 10 μm. (**B**) CGNs were cultured for 24 h with (filled bars) or without (open bars) MAG–Fc. The cells were treated with K252a 15 min before the end of the incubation period with MAG–Fc. (**C**) siRNA-mediated knockdown of endogenous TrkB attenuated the effects of MAG–Fc on neurite growth. The neurons transfected with control siRNA, TrkB siRNA #1, or TrkB siRNA #2 were cultured for 24 h in the presence or absence of MAG–Fc. Western blot analysis for TrkB in the transfected cells (lower panels). Tubulin: Tuj1. (**D**) CGNs were treated with fluorescein isothiocyanate (FITC)-conjugated TAT–TrkA 484–497 for 30 min, and the presence of the peptide in the cells was assessed. (**E**) TAT–TrkA 484–497 blocked association of TrkB with SHP-2. CGNs were pretreated with 10 μM TAT–TrkA 484–497 for 15 min and then incubated with MAG–Fc for 15 min. Co-immunoprecipitation was performed. (**F, G**) The TAT-fused peptides blocked the neurite growth inhibition induced by MAG–Fc. CGNs were pretreated with 1 or 10 μM TAT–TrkA 484–497 (**F**) or TAT–TrkA 481–494 (**G**) for 15 min, followed by incubation with MAG–Fc for 24 h. (**A–G**) *$P<0.05$, **$P<0.01$. A full-colour version of this figure is available at *The EMBO Journal* Online.

Figure 4 Inhibition of endogenous SHP reduces MAG-induced dephosphorylation of TrkB. (**A**) Stimulation with MAG reduced the tyrosine phosphorylation levels of Trk receptors. CGNs were left untreated or treated with 25 μg/ml MAG–Fc for 30 min in the presence or absence of 100 ng/ml BDNF during the final 5 min. Cell lysates were immunoprecipitated with anti-pan Trk antibodies. The immunoprecipitates (IP) were analysed by immunoblotting with anti-phospho Tyr and anti-Trk antibodies. The phosphorylation level of Trk receptors was determined by western blotting (WB: pTyr). (**B**) SHP inhibition suppressed MAG–Fc-induced dephosphorylation of Trk receptors in CGNs. CGNs were pretreated with NSC-87877 for 3 h and left untreated or stimulated with MAG–Fc as in (**A**). (**C, D**) Knockdown of SHP attenuated MAG–Fc-induced dephosphorylation of Trk receptors in CGNs. CGNs were transfected with SHP-1 (**C**), SHP-2 (**D**), or control siRNAs; 72 h after transfection, CGNs were left untreated or treated with MAG–Fc for 30 min. The right panels show that the expressions of SHP-1 (**C**) and SHP-2 (**D**) were decreased by transfection of the corresponding siRNAs. (**E, F**) Knockdown of SHP suppressed MAG–Fc-induced dephosphorylation of TrkB in retinal cells. Retinal cells were transfected with SHP-1 (**E**), SHP-2 (**F**), or control siRNAs. Knockdown of SHP-1 or SHP-2 per se significantly increased TrkB phosphorylation and attenuated the effects of MAG–Fc. (**G**) PIR-B is required for the MAG-induced dephosphorylation of TrkB. CGNs from WT and PIR-B KO mice were stimulated with MAG–Fc (25 μg/ml) for 30 min. (**H**) p75 is required for MAG-induced dephosphorylation of TrkB. CGNs from WT and p75-deficient mice were stimulated with MAG–Fc and BDNF. Lysates were precipitated with anti-Trk antibodies before detection with anti-phospho Tyr antibodies. (**A–H**) The graphs present the data from three independent experiments. *$P<0.05$, **$P<0.01$.

the effect of MAG on the CGNs (Figure 3D and E). Double knockdown of SHP-1 and SHP-2 completely suppressed the effect (Figure 5A). Thus, we consider that both SHP-1 and SHP-2 are necessary for MAG–Fc-induced neurite growth inhibition. Because SHP-1 and SHP-2 inhibit Trk activity, these results suggest that the basal activity of Trk receptors contributes to CGN neurite growth. MAG may inhibit neurite growth by lowering this basal activity, because no neurotrophins were added to the culture medium. To examine this hypothesis, K252a, a pan Trk inhibitor, was added to the culture medium 15 min before adding MAG, and the effect of MAG–Fc was assessed (Figure 5B). K252a mimicked the effect of MAG–Fc and significantly inhibited neurite growth. MAG–Fc did not further reduce neurite growth in K252a-treated CGNs. To rule out possible non-specific effects of this inhibitor, TrkB was knocked down by siRNA (Figure 5C, lower panels). Knockdown of TrkB significantly blocked neurite growth inhibition in CGNs and prevented MAG–Fc-induced activities (Figure 5C). These results confirmed that MAG reduces the basal activity of TrkB and inhibits neurite growth in CGNs. Finally, we determined whether the association of SHP-1/2 with TrkB is necessary for the inhibitory effect of MAG–Fc. A previous study has reported that SHP-1 interacts with TrkA at Y490 and dephosphorylates it at Y674/675 (Marsh et al, 2003). Based on this knowledge, we generated two TrkA peptides containing a 14-amino acid sequence comprising Y490. We then examined whether these peptides inhibit PIR-B signaling by blocking the SHP-1/2–Trk receptor interaction. To allow entrance into the cell in order to directly act on SHP-1/2 in vivo, the peptides were fused with the amino-terminal protein transduction domain (11 amino acids) from the human immunodeficiency virus (HIV) protein transactivator protein TAT (Schwarze et al, 1999) (TAT–TrkA 484–497 and TAT–TrkA 481–494). As expected, both peptides entered the CGNs efficiently within 30 min of addition (Figure 5D; only data from TAT–TrkA 484–497 are shown), and blocked the association of TrkB with SHP-2 (Figure 5E; only data from TAT–TrkA 484–497 are shown) and SHP-1 (data not shown). The addition of 1 μM TAT–TrkA 484–497 (Figure 5F) or 1 μM TAT–TrkA 481–494 (Figure 5G) to the CGN culture reduced the inhibitory effect of MAG–Fc on neurite growth. These results suggested that binding of SHP-1/2 to TrkB is critical for MAG signal transduction.

Knockdown of SHP promotes optic nerve regeneration

We assessed whether PIR-B signaling inhibition enhances axonal regeneration in the CNS. For this purpose, we employed the optic nerve crush injury model in mice. In vivo siRNA transfection was conducted to inhibit SHP-1 or SHP-2 in retinal cells, which expressed both SHP-1 and SHP-2

(Figure 6A). Efficient transfection of Alexa488-labeled siRNA in the retina was achieved (Figure 6B). These animals were subjected to optic nerve injury. The lysates were prepared from eye cups at 5, 11, and 14 days after injection of siRNA (Figure 6C), and the expression of each SHP isoform was examined by western blotting. The results demonstrated that the silencing effect persisted for at least 5–14 days. After in vivo transfection of SHP-1 (Figure 6D) or SHP-2 (Figure 6E) siRNA, the dissociated retinal cells were obtained and stimulated with MAG–Fc. Knockdown of SHP-1 (Figure 6D) or SHP-2 (Figure 6E) resulted in reduced MAG–Fc-induced dephosphorylation of TrkB. Knockdown of either isoform by itself enhanced the TrkB phosphorylation. These in vivo results were consistent with our above-mentioned in vitro findings. MAG–Fc-induced dephosphorylation of TrkB was reduced also in retinal cells from PIR-B$^{-/-}$ mice, whereas the basal level of TrkB phosphorylation was not enhanced in these cells (Figure 6F).

To assess axonal regeneration, the axons of the injured optic nerve were traced by injecting Alexa555-conjugated cholera toxin β subunit (CTB) into the vitreous humour (Figure 7A and C). The results revealed that in vivo optic nerve regeneration was significantly promoted by transfection of either SHP-1 siRNA or SHP-2 siRNA as compared with control siRNA, albeit the small number of regenerating axons in the optic nerve (Figure 7B and D). Thus, silencing of SHP-1 and SHP-2 contributed to the regeneration of injured axons in the optic nerve. Next, we used PIR-B$^{-/-}$ mice to determine the role of PIR-B in axon regeneration. In PIR-B$^{-/-}$ mice, the number of regenerating axons was comparable to that seen in WT mice (Figure 7E). Because downregulation of SHP-1 or SHP-2 per se enhanced TrkB phosphorylation (Figure 6D and E), we reasoned that activation of TrkB as well as inhibition of PIR-B may be necessary for axonal regeneration. Indeed, the basal level of TrkB phosphorylation was not enhanced in retinal cells from PIR-B$^{-/-}$ mice (Figure 6F). To test this hypothesis, we injected BDNF into the eyes of PIR-B$^{-/-}$ mice. Interestingly, BDNF injection increased axonal regeneration in PIR-B$^{-/-}$ mice but not in WT mice (Figure 7E and F). These results suggested that inhibition of PIR-B and activation of Trk receptors are necessary for axonal regeneration.

Discussion

We proposed the following molecular model for PIR-B signal transduction: first, PIR-B associates with Trk receptors, inactivating them (Figure 8); second, binding of MAG to PIR-B leads to the association of PIR-B with Trk receptors; third, SHP-1 and SHP-2, which are recruited to PIR-B upon MAG


Figure 6 In vivo knockdown of SHP-1 or SHP-2 in mouse retinas. (**A**) Immunohistochemical staining of SHP-1 and SHP-2 in mouse retinas. The nuclei were stained by DAPI. Scale bar: 50 μm. GCL, ganglion cell layer; INL, inner nuclear layer; ONL, outer nuclear layer. (**B**) Distribution of Alexa488-labeled siRNA in the retina after intravitreous injection. Alexa488-labeled siRNA was localized to the ganglion cells. (**C**) Western blots showing downregulation of each SHP isoform after siRNA injection. Optic nerve extracts were prepared from mice injected with control, SHP-1 #1/#2, or SHP-2 #1/#2 siRNA. At 5, 11, and 14 days after siRNA injection, lysates were prepared from the eye with the nerve segment. Representative blots from the sample prepared at 11 days after siRNA injection are shown. The signal intensity was quantified by densitometry and normalized to tubulin levels. The relative SHP-1 or SHP-2 protein levels are shown in the graphs. (**D**, **E**) In vivo knockdown of SHP suppressed MAG–Fc-induced dephosphorylation of Trk receptors in retinal cells. Optic nerve extracts were prepared from the eyes injected with SHP-1 (**D**), SHP-2 (**E**), or control siRNA, and the phosphorylation level of TrkB was determined by immunoblotting of the precipitated TrkB. (**F**) Retinal cells were prepared from WT and PIR-B$^{-/-}$ mice. The cells were stimulated with or without MAG–Fc. (**C–F**) **$P < 0.01$, *$P < 0.05$.

stimulation, are required for the effects of MAG on neurite growth inhibition and TrkB dephosphorylation. Thus, PIR-B negatively regulates the basal and/or neurotrophin-regulated levels of Trk activity through SHP-1/2 in postnatal CGNs.

Our findings suggest that a balance in the expression of Trk receptors and PIR-B is critical for the potential of axonal growth following injury. Trk receptors activate key survival and axonal growth regulatory proteins, such as phosphatidy-linositol 3-kinase, Akt, and mitogen-activated protein kinase
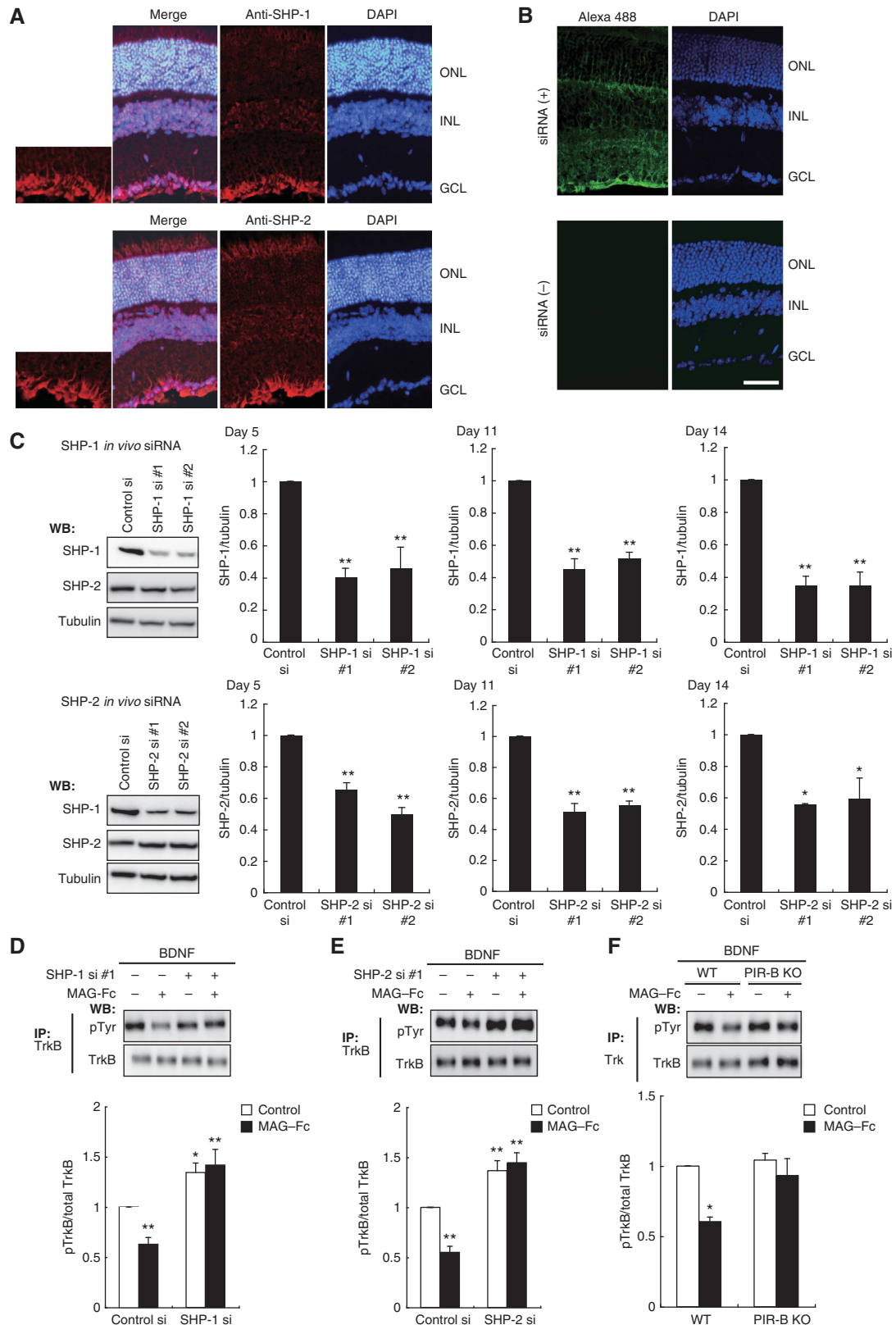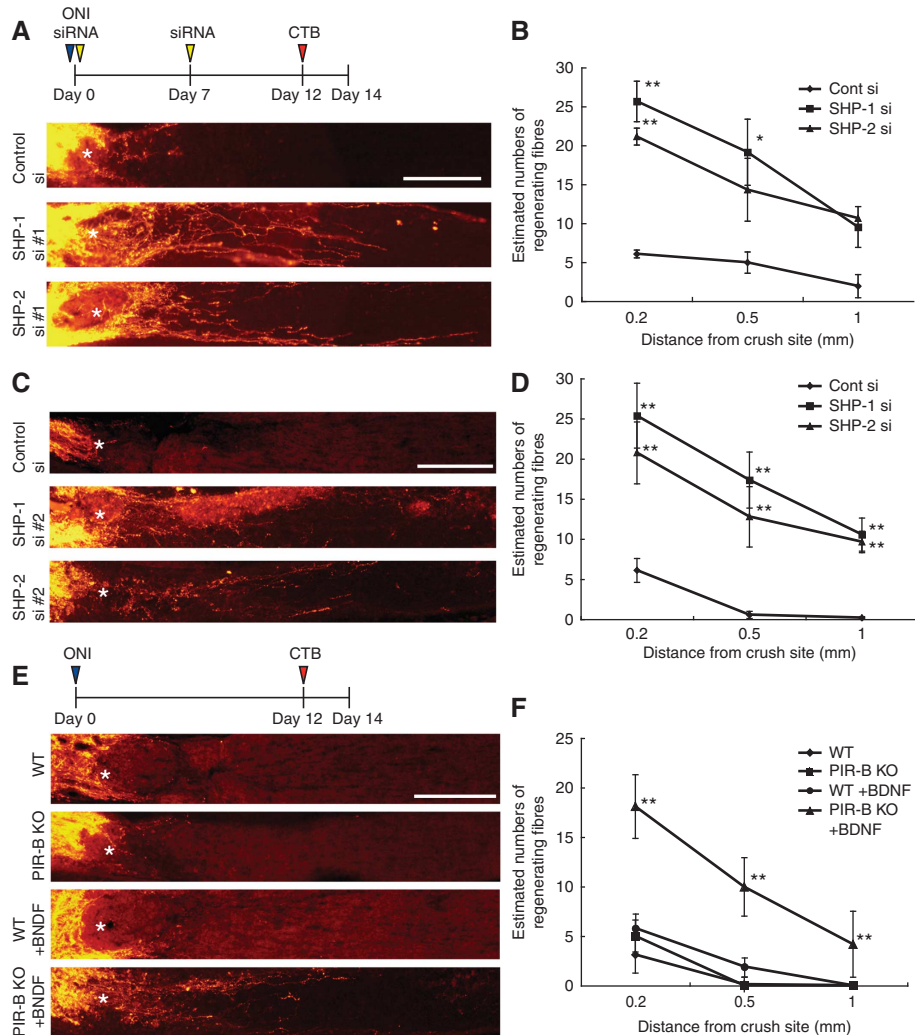
Figure 7 *In vivo* transfection of siRNAs against SHP results in enhanced axonal regeneration. (**A**) Confocal micrographs of optic nerve axons labeled by CTB at 14 days after axotomy. *In vivo* transfection with control siRNA (control si), SHP-1 siRNA #1 (SHP-1 si #1), or SHP-2 siRNA #1 (SHP-2 si #1) was performed. *Injury site. Scale bar: 200 μm. (**B**) Quantitative analysis of regenerating axons extending 0.2, 0.5, and 1.0 mm from the end of the crush site at 14 days after injury. At least five different sections per animal were quantified. Significant differences were found between the control ($N = 6$) and the other two groups (SHP-1 si #1 ($N = 6$)]and SHP-2 si #1 ($N = 7$)). (**C, D**) The results were confirmed using different siRNA sets. $N = 6$ (control), 7 (SHP-1 siRNA #2 (SHP-1 si #2), and 6 (SHP-2 siRNA #2 (SHP-2 si #2)). (**E**) Longitudinal sections through the optic nerve showing CTB-labeled axons distal to the injury site in WT mice, PIR-B KO mice, and WT mice or PIR-B KO mice treated intravitreally with BDNF 14 days after injury. *Injury site. Scale bar: 200 μm. (**F**) Quantitative analysis of regenerating axons at 14 days after injury. $N = 6$ (WT), 6 (PIR-B KO), 6 (WT + BDNF), and 8 (PIR-B KO + BDNF). **$P < 0.01$. (**B, D, F**) *$P < 0.05$, **$P < 0.01$.

(Kaplan and Miller, 2000; Patapoutian and Reichardt, 2001). Although these signals are activated by binding of neurotrophins to Trk receptors, the basal activity of Trk receptors in the absence of ligand binding may also be important. It has been suggested that SHP-1 is a regulator of basal TrkA activity, because inhibition of endogenous SHP-1 stimulates basal tyrosine phosphorylation of TrkA, thereby promoting the survival of sympathetic neurons and PC12 cells during NGF withdrawal (Marsh *et al*, 2003). Conversely but consistently, our data suggest that the basal Trk receptor activity is reduced by increased binding of SHP-1/2 to Trk receptors, resulting in neurite growth inhibition. This effect may be independent of neurotrophins, because no neurotrophins were added to the culture during the neurite growth assay performed in the present study. Furthermore, BDNF could not be detected in the CGN culture medium (data not shown). Nonetheless, growth of neurites < 40 μm in average

(Figure 5B and C) may not reflect the crucial role of TrkB in MAG-induced neurite growth inhibition but rather the general importance of TrkB to neurite growth, which cannot be inhibited further.

The SHP family of protein tyrosine phosphatases includes SHP-1, SHP-2, and the *Drosophila melanogaster* homologue Corkscrew (Tonks and Neel, 2001). SHP-1 is expressed in the haematopoietic system, the nervous system, epithelial cells, and the NGF-responsive PC12 cell line (Tonks and Neel, 2001). SHP-1 has been shown to interact with and dephosphorylate several growth factor receptors, including IGF-1, PDGF, EGF (Tonks and Neel, 2001), and TrkA (Marsh *et al*, 2003). It has been shown that SHP-1 acts as a TrkA phosphatase in PC12 cells and sympathetic neurons *in vitro* and *in vivo* and that it maintains low levels of basal TrkA activation and attenuates long-term TrkA signaling in the presence of NGF (Marsh *et al*, 2003). Further, an enhanced
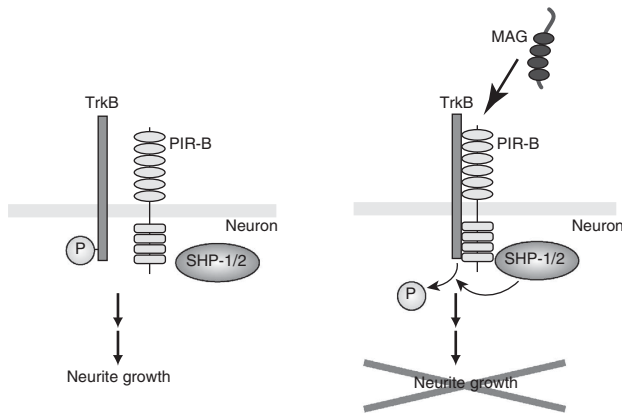
Figure 8 Proposed molecular model of the PIR-B signal transduction. Ligand binding to PIR-B leads to the formation of a receptor complex composed of PIR-B and TrkB. SHP-1/2, which is recruited to PIR-B, interacts with and deactivates TrkB by tyrosine dephosphorylation, causing neurite outgrowth inhibition.

association of SHP-2 with TrkB inhibits BDNF-induced TrkB autophosphorylation and activation in postnatal CGNs (Rusanescu et al, 2005). Considering that SHP-1 and SHP-2 negatively regulate Trk activity, the balancing mechanism between Trk receptors and PIR-B may determine the potential of axonal regeneration of the injured CNS through SHP-1 and SHP-2. Further, our observation may be relevant to the development of the nervous system if activation of the basal and/or neurotrophin-dependent Trk activities through PIR-B inhibition contributes to extension of the critical period.

NgR is another receptor for MAG, Nogo, and OMgp. The combination of NgR-null cerebellar neurons and function-blocking PIR-B antibodies has been reported to completely overcome inhibition by myelin (Atwal et al, 2008). This implies that the putative third receptor has no role in transducing signals mediated by myelin. It would be interesting to assess the possible cross talk of the downstream signals mediated by PIR-B and NgR. The small guanine nucleoside triphosphatase RhoA has been previously shown to act downstream of NgR as a key intracellular effector of neurite growth inhibition induced by myelin (Yiu and He, 2006). In its active GTP-bound form, RhoA rigidifies the actin cytoskeleton, thereby inhibiting axonal elongation and mediating growth cone collapse. RhoA, which is activated by these proteins, inhibits neurite outgrowth from the postnatal sensory neurons and CGNs (Yiu and He, 2006). In addition, conventional protein kinase C and the EGF receptor are also involved in the inhibitory effect (Yiu and He, 2006). These multiple signals are found downstream of NgR, and they are responsible for the effect of myelin-derived inhibitors. Interestingly, our present data show that inhibition of SHP-1/2 totally abolished the inhibitory effects of MAG on neurons (dephosphorylation of Trk receptors and neurite growth inhibition by MAG–Fc), whereas the inhibition of PIR-B partially reduced the effects. Thus, SHP may be required not only for PIR-B signaling but also for NgR signaling.

Importantly, our data show that inhibition of SHP signaling enhanced axonal regeneration in the injured optic nerve in mice, yet the number of regenerating axons in the optic nerve was fairly reduced. Therefore, SHP may be a new molecular target for treating CNS injuries. Recently, it has been shown

that triple-mutant mice that lack MAG, Nogo, and OMgp fail to exhibit any enhancement in the regeneration or functional recovery after spinal cord injury in comparison with WT mice (Lee et al, 2010). This report suggests that inhibition of the three myelin inhibitors may be insufficient for axonal regeneration in the CNS. Furthermore, we observed no enhancement in axonal regeneration after spinal cord injury in PIR-B$^{-/-}$ mice (Nakamura et al, 2011). However, it should be noted that targeting conventional protein kinase C and the EGF receptor as well as RhoA/Rho-kinase promotes axonal regeneration in the injured CNS (Yiu and He, 2006), which is in agreement with our findings on SHP inhibition. One possible explanation for the inconsistency is that the inhibition of SHP or other intracellular signaling molecules may enhance the intrinsic regenerative response in vivo, as Trk activity is induced by silencing SHP. Elucidation of the possible cross talk between myelin signaling and the molecular mechanisms underlying the regenerative response may help clarify the seemingly contradictory findings in this field.

In summary, we dissected the PIR-B signaling cascade responsible for neurite growth inhibition in CGNs and demonstrated the involvement of MAG and Trk receptors. Further, we showed that knockdown of SHP-1 and SHP-2 induced axonal regeneration during CNS injury in mice. We suggest SHP-1 and SHP-2 as potential therapeutic targets for nerve regeneration in CNS injury.

Materials and methods

Animals
We purchased C57BL/6J mice from Charles River Laboratories. These mice were bred and maintained in the Institute of Experimental Animal Sciences at the Osaka University Graduate School of Medicine. PIR-B$^{-/-}$ mice were generated as previously described (Ujike et al, 2002) and backcrossed to C57BL/6J mice. We used a C57BL/6J mouse strain bearing a targeted disruption of the third exon of the p75 gene (Lee et al, 1992), which was obtained from the Jackson Laboratory (Bar Harbor, Maine). All experimental procedures were approved by the Institutional Committee of the Osaka University.

Reagents and antibodies
The following reagents were used in this study: purified MAG–Fc (25 µg/ml), recombinant BDNF (100 ng/ml; Peprotech, Rocky Hill, NJ, USA), NSC-87877 (50 µM; Calbiochem, San Diego, CA, USA), and K252a (100 nM; Alomone Labs, Jerusalem, Israel). The TAT–TrkA 481–494 (TAT–QGHIIENPQYFSDA), TAT–TrkA 484–497 (TAT–IIENPQYFSDACVH), and TAT-fused control (TAT–HVCAES-FYQPNEII) peptides were chemically synthesized (Sigma-Aldrich, St Louis, MO, USA). Stable CHO cell lines secreting human MAG–Fc were provided by Endo M (Kobe University). The cells were cultured in serum-free medium. Conditioned medium was collected after 3 days, and MAG–Fc was purified with protein A Sepharose beads. For immunoprecipitation, western blotting, and immunostaining the following antibodies were used: monoclonal anti-HA (HA-7, 1:5000; Sigma-Aldrich), anti-c-Myc (9E10, 1:1000; Santa Cruz Biotechnology, CA, USA), biotinylated anti-TrkB (1:2500; R&D systems), anti-SHP-1 (1:1000; BD Transduction Laboratories, San Jose, CA, USA), anti-SHP-2 (1:1000, BD Transduction Laboratories), anti-MAG (1:200; Santa Cruz Biotechnology, Millipore), anti-α-tubulin (1:1000; Santa Cruz Biotechnology), and anti-neuronal class III β-tubulin (Tuj1, 1:5000; Covance Laboratories, Inc., Berkeley, CA, USA); polyclonal anti-SHP-1, anti-SHP-2, anti-Trk, anti-TrkB, anti-PIR-B (1:1000; Santa Cruz Biotechnology), anti-phospho TrkB (1:500 Cell Signaling Technology, Danvers, MA, USA), anti-PIR-B (1 mg/ml; R&D systems), and anti-PIR-A/B (1:1000; BD Pharmingen, San Diego, CA, USA); secondary horseradish peroxidase (HRP)-conjugated anti-mouse, anti-rabbit, or anti-rat IgG (Cell Signaling Technology), HRP-conjugated anti-goat IgG (Santa Cruz

Biotechnology), streptavidin-peroxidase (Roche Applied Science, Indianapolis, IN, USA), and Alexa488- or 568-conjugated goat anti-mouse IgG (Molecular Probes, Eugene, OR, USA).

Plasmid constructs and siRNA

Pir-b was subcloned into the pcDNA3.1Zeo(+) vector as previously described (Endo *et al*, 2008). TrkB constructs were provided by Barde YA (Bibel *et al*, 1999). The mammalian expression vectors encoding human TrkA (Addgene plasmid 15002) (Yano *et al*, 2001), human SHP-1 (Addgene plasmid 8572), and SHP-2 (Addgene plasmid 8381) were all obtained from Addgene (Cambridge, MA, USA). The following siRNAs were used for knockdown experiments: mouse SHP-1 and mouse SHP-2 (ON-TARGETplus SMARTpool; Thermo Fisher Scientific, Dharmacon Products, Lafayette, CO, USA), and mouse NTRK2 (stealth siRNA; Invitrogen). The ON-TARGET plus SMARTpool siRNA is a mixture of four individual siRNA duplexes. Alexa 488-labeled siRNAs were chemically synthesized (Invitrogen) and contained the following sequences: SHP-1 #1-sense AF488 (5'-GACUGUGACAUUGAUAUC CAGAAGA-3'), SHP-1 #1-antisense (5'-UCUUCUGGAUAUCAAUGU CACAGUC-3'), SHP-1 #2-sense AF488 (5'-CAGCAGAAUACAAACUG CGAACAUU-3'), SHP-1 #2-antisense (5'-AAUGUUCGCAGUUUGUAU UCUGCUG-3'), SHP-2 #1-sense AF488 (5'-CCACUUUGGCUGAACUG GUUCAGUA-3'), SHP-2 #1-antisense (5'-UACUGAACCAGUUCAGC CAAAGUGG-3'), SHP-2 #2-sense AF488 (5'-CCUCUGAAAGGUGGU UCCAUGGUCA-3'), and SHP-2 #1-antisense (5'-UGACCAUGGAACC ACCUUUCAGAGG-3'). As mismatch control, single base pair changes were introduced in the SHP-1 and SHP-2 siRNAs.

Cell culture

COS-7 cells were cultured in Dulbecco's modified Eagle's medium (DMEM; Invitrogen) containing 10% fetal bovine serum (FBS). Transient transfection of COS-7 cells was performed using Lipofectamine 2000 (Invitrogen) according to the manufacturer's instructions. The cells were lysed 24–48 h after transfection and used for immunoprecipitation. Primary dissociated cultures of CGNs from P7 mice were prepared as previously reported (Hata *et al*, 2009). In brief, cells were gently dissociated after digestion with 0.25% trypsin (Gibco/Invitrogen, Paisley, UK) and DNase1 (Takara, Shiga, Japan) at 37°C for 15 min. DMEM/F12 containing 10% FBS was added, and the cells were centrifuged at 1000 r.p.m. for 3 min. The neurons were then plated on poly-L-lysine-coated dishes and maintained in DMEM/F12 supplemented with B27 (Invitrogen) at 37°C with 5% CO_2. After 24 h, the medium was replaced with DMEM/F12 containing 0.1% bovine serum albumin (BSA). After 24-h incubation, the neurons were harvested for immunoprecipitation or western blotting. For dissociated retinal cell cultures, P7–P9 mice were used. Eyes were enucleated, and retinas were dissected and incubated at 37°C for 30 min in a digestion solution containing papain (16.5 U/ml; Worthington Biochem., NJ, USA), DNase (0.5 mg/ml; Sigma), and L-cysteine (0.3 g/ml, Sigma) in phosphate-buffered solution (PBS). Cells were then rinsed with DMEM containing 10% FBS and centrifuged at 1000 r.p.m. for 5 min. To remove cell debris, the cell suspension was passed through a cell strainer (70 µm; BD Falcon, Franklin Lakes, NJ). After centrifugation, the supernatant was discarded and the cells were carefully resuspended in DMEM supplemented with B27 (1:50; Invitrogen) or subjected to nucleofection.

Nucleofection

CGNs and retinal neurons were isolated and dissociated from P7 to P9 mice as described above. The cells were washed and resuspended in room temperature Mouse Neuron Nucleofector Solution (Amaxa; Lonza Cologne AG, Cologne, Germany) at a final concentration of 5×10^6 cells per 100 µl. The cell–nucleofector solution complex (100 µl) and the various siRNA duplexes or control non-targeting siRNA (500 pmol) were then gently mixed and transferred into a cuvette, followed by nucleofection using the nucleofector program O-05. Immediately after electroporation, the cells were mixed with 500 µl of pre-warmed DMEM/F12 containing 10% FBS, and the cell suspension was then transferred onto poly-L-lysine-coated dishes. The cells were placed in an incubator for 3 h, after which the medium was replaced by fresh DMEM/F12 containing B27, and the cells were incubated for an additional 48–72 h. The cells were then transferred to serum-free conditions for immunoprecipitation or western blotting, or collected

and plated onto poly-L-lysine-coated dishes for the neurite outgrowth assay.

Co-immunoprecipitation

Cells were washed with ice-cold PBS and lysed on ice in lysis buffer containing 50 mM Tris–HCl (pH 7.4), 150 mM NaCl, 0.5–1% NP-40, 10 mM NaF, 1 mM Na_3VO_4, and a protease inhibitor cocktail (Roche Diagnostics K.K., Tokyo, Japan), followed by centrifugation at 4°C at 15 000 r.p.m. for 10 min. The supernatants were incubated with the indicated antibodies for 2 h or overnight at 4°C. Mouse brains were homogenized in lysis buffer containing 50 mM Tris–HCl (pH 7.5), 150 mM NaCl, 1 mM EDTA, 1.0% NP-40, and a protease inhibitor cocktail (Roche Diagnostics KK). The lysates were centrifuged at $17 000 \times g$ at 4°C for 15 min and incubated with protein G Sepharose at 4°C for 1 h to reduce non-specific binding to the beads. Cleared lysates were collected and incubated with anti-PIR-B antibodies. The immune complexes were collected after incubation for 1 h at 4°C with protein A Sepharose, protein G Sepharose (GE Healthcare, Chalfont St Giles, England), or streptavidin agarose beads (Thermo Scientific) that had been pre-coated with 0.1–0.5% BSA. After washing the beads three times with the lysis buffer, the proteins were eluted by boiling in 25 µl of 2 × sample buffer for 5 min and subjected to sodium dodecyl sulphate polyacrylamide gel electrophoresis (SDS–PAGE), followed by western blotting. Where indicated, the cells were treated with 25 µg/ml MAG–Fc or recombinant human IgG–Fc (R&D systems).

Western blotting

Cell lysates were boiled in sample buffer for 5 min. The proteins were separated by SDS–PAGE and transferred onto polyvinylidene difluoride (PVDF) membranes (Millipore). The membrane was blocked with 5% non-fat dry milk in PBS containing 0.05% Tween-20 (PBS-T) and incubated for 1 h at room temperature or overnight at 4°C, with the primary antibody diluted in PBS-T containing 1% non-fat dry milk. After washing in PBS-T, the membrane was incubated with an HRP-conjugated anti-mouse IgG, anti-rabbit IgG antibody (Cell Signaling Technology), or streptavidin–POD (Roche Applied Science). For detection, an ECL chemiluminescence system (GE Healthcare) was used. Signals were detected and quantified using the LAS-3000 image analyzer (Fuji Film, Tokyo, Japan).

RNA extraction, reverse transcription, and real-time PCR

Total RNA was extracted from CGNs with Trizol (Invitrogen) and reverse transcribed using the High-Capacity cDNA Reverse Transcription Kit (Applied Biosystems, Foster City, CA, USA). mRNA expression was determined by real-time PCR using a 7300 fast real-time PCR system (Applied Biosystems). TaqMan assays (Applied Biosystems) were used to quantitate SHP-1 (Mm00469153_m1) and SHP-2 (Mm 00448434_m1) using the TaqMan Gene Expression Master Mix (Applied Biosystems). The relative mRNA expression was calculated after normalization to the expression of glyceraldehyde 3-phosphate dehydrogenase mRNA. The results of cycle threshold values (Ct values) were calculated by the ΔΔCt method to obtain the fold differences.

Neurite outgrowth assay

Neurite outgrowth assay was performed as described previously (Hata *et al*, 2006). In brief, CGNs were left untreated or were treated with MAG–Fc in DMEM/F12 medium for 24 h. Then, cells were fixed with 4% (w/v) paraformaldehyde (PFA) and immunostained with an anti-TuJ1 monoclonal antibody.

Optic nerve injury, in vivo siRNA transfection, and anterograde labeling

Optic nerve injury was performed as previously described in detail (Smith *et al*, 2009). The left optic nerve of P21 mice was exposed intraorbitally and crushed with fine forceps for 10 s at ~1 mm from the optic disc. Then, intravitreal injections were performed with a pulled glass pipette affixed to a Hamilton syringe. Care was taken not to damage the lens. The animals were divided into different experimental conditions: control siRNA, SHP-1 siRNA, SHP-2 siRNA (1.5 µg/µl), BDNF (5 µg/µl), or control (an equivalent volume of PBS). The second injection was administered 1 week after axotomy. On day 12 after axotomy, 1 µl Alexa555-conjugated CTB (2 µg/µl; Invitrogen) was injected into the vitreous with a glass needle. On day 14 after axotomy, the animals received an overdose of anaesthesia followed by perfusion with 4% PFA. The

eyes were enucleated. The lens and the vitreous body were removed, and the remaining eyecup with the nerve segment was post-fixed in 4% PFA for 12 h at 4°C. The eyecups were then dehydrated in 10–30% sucrose overnight at 4°C and immersed in Optimal Cutting Temperature compound (Tissue Tek). Tissues were frozen in dry ice and serial cross sections (16 µm) were prepared using a cryostat and collected on MAS-coated glass slides.

Immunohistochemistry

Cryostat sections were incubated with blocking solution containing 5% BSA and 0.1–0.2% Triton X-100 in PBS for 1 h at room temperature, followed by overnight incubation with the appropriate antibodies at 4°C. Immunoreactivity was visualized using fluorescence-conjugated secondary antibodies. Coverslips were then mounted with mounting medium.

Quantification of axonal regeneration

Images were acquired on a microscope (BX51; Olympus) equipped with a camera (DP71; Olympus) using the DP Controller software (version 3.1.1.267; Olympus). Axonal regeneration was quantified by counting the number of CTB-labeled axons extending 0.2, 0.5, and 1.0 mm from the end of the crush site in five different sections. The cross-sectional width of the nerve was measured at the point at which the counts were taken and was used to calculate the number of axons per millimetre of nerve width. The number of axons per millimetre was then averaged over the five sections. $\sum ad$, the total number of axons

extending the distance d in a nerve having a radius of r, was estimated by summing all the sections having a thickness t (16 µm):

$$\sum ad = \pi r^2 \times (\text{average axons/mm})/t$$

Statistical analysis

The data are presented as the mean ± s.e.m. of 3 independent experiments. Statistical analyses were performed using Welch's *t*-test (Figures 1H, 2A, C and D), one-way ANOVA, followed by Scheffe's (Figures 3A–E, 4F, 5A–C, 6C, 7D and F), Holm's (Figures 4A–E, G, H, 5F, G and 6D–F) or Bonferroni's (Figure 7B) multiple comparison test. *P*-values of <0.05 were considered significant.

Acknowledgements

Conflict of interest

The authors declare that they have no conflict of interest.

References

Atwal JK, Pinkston-Gosse J, Syken J, Stawicki S, Wu Y, Shatz C, Tessier-Lavigne M (2008) PirB is a functional receptor for myelin inhibitors of axonal regeneration. *Science* **322**: 967–970

Bibel M, Hoppe E, Barde YA (1999) Biochemical and functional interactions between the neurotrophin receptors trk and p75NTR. *EMBO J* **18**: 616–622

Endo S, Sakamoto Y, Kobayashi E, Nakamura A, Takai T (2008) Regulation of cytotoxic T lymphocyte triggering by PIR-B on dendritic cells. *Proc Natl Acad Sci USA* **105**: 14515–14520

Hata K, Fujitani M, Yasuda Y, Doya H, Saito T, Yamagishi S, Mueller BK, Yamashita T (2006) RGMa inhibition promotes axonal growth and recovery after spinal cord injury. *J Cell Biol* **173**: 47–58

Hata K, Kaibuchi K, Inagaki S, Yamashita T (2009) Unc5B associates with LARG to mediate the action of repulsive guidance molecule. *J Cell Biol* **184**: 737–750

Kaplan DR, Miller FD (2000) Neurotrophin signal transduction in the nervous system. *Curr Opin Neurobiol* **10**: 381–391

Lee JK, Geoffroy CG, Chan AF, Tolentino KE, Crawford MJ, Leal MA, Kang B, Zheng B (2010) Assessing spinal axon regeneration and sprouting in Nogo-, MAG-, and OMgp-deficient mice. *Neuron* **66**: 663–670

Lee KF, Li E, Huber LJ, Landis SC, Sharpe AH, Chao MV, Jaenisch R (1992) Targeted mutation of the gene encoding the low affinity NGF receptor p75 leads to deficits in the peripheral sensory nervous system. *Cell* **69**: 737–749

Marsh HN, Dubreuil CI, Quevedo C, Lee A, Majdan M, Walsh GS, Hausdorff S, Said FA, Zoueva O, Kozlowski M, Siminovitch K, Neel BG, Miller FD, Kaplan DR (2003) SHP-1 negatively regulates neuronal survival by functioning as a TrkA phosphatase. *J Cell Biol* **163**: 999–1010

Nakamura Y, Fujita Y, Ueno M, Takai T, Yamashita T (2011) Paired immunoglobulin-like receptor B knockout does not enhance axonal regeneration or locomotor recovery after spinal cord injury. *J Biol Chem* **286**: 1876–1883; PMID: 21087927

Patapoutian A, Reichardt LF (2001) Trk receptors: mediators of neurotrophin action. *Curr Opin Neurobiol* **11**: 272–280

Rusanescu G, Yang W, Bai A, Neel BG, Feig LA (2005) Tyrosine phosphatase SHP-2 is a mediator of activity-dependent neuronal excitotoxicity. *EMBO J* **24**: 305–314

Schwarze SR, Ho A, Vocero-Akbani A, Dowdy SF (1999) *In vivo* protein transduction: delivery of a biologically active protein into the mouse. *Science* **285**: 1569–1572

Smith PD, Sun F, Park KK, Cai B, Wang C, Kuwako K, Martinez-Carrasco I, Connolly L, He Z (2009) SOCS3 deletion promotes optic nerve regeneration *in vivo*. *Neuron* **64**: 617–623

Syken J, Grandpre T, Kanold PO, Shatz CJ (2006) PirB restricts ocular-dominance plasticity in visual cortex. *Science* **313**: 1795–1800

Takai T (2005) Paired immunoglobulin-like receptors and their MHC class I recognition. *Immunology* **115**: 433–440

Tonks NK, Neel BG (2001) Combinatorial control of the specificity of protein tyrosine phosphatases. *Curr Opin Cell Biol* **13**: 182–195

Ujike A, Takeda K, Nakamura A, Ebihara S, Akiyama K, Takai T (2002) Impaired dendritic cell maturation and increased T(H)2 responses in PIR-B(−/−) mice. *Nat Immunol* **3**: 542–548

Wang KC, Kim JA, Sivasankaran R, Segal R, He Z (2002) P75 interacts with the Nogo receptor as a co-receptor for Nogo, MAG and OMgp. *Nature* **420**: 74–78

Yamashita T, Higuchi H, Tohyama M (2002) The p75 receptor transduces the signal from myelin-associated glycoprotein to Rho. *J Cell Biol* **157**: 565–570

Yano H, Lee FS, Kong H, Chuang J, Arevalo J, Perez P, Sung C, Chao MV (2001) Association of Trk neurotrophin receptors with components of the cytoplasmic dynein motor. *J Neurosci* **21**: RC125

Yiu G, He Z (2006) Glial inhibition of CNS axon regeneration. *Nat Rev Neurosci* **7**: 617–627

Zheng B, Atwal J, Ho C, Case L, He XL, Garcia KC, Steward O, Tessier-Lavigne M (2005) Genetic deletion of the Nogo receptor does not reduce neurite inhibition *in vitro* or promote corticospinal tract regeneration *in vivo*. *Proc Natl Acad Sci USA* **102**: 1205–1210